Generalized Vortex Lattice Method for Predicting Characteristics of Wings with Flap and Aileron Deflection

Mondher Yahyaoui

Abstract—A generalized vortex lattice method for complex lifting surfaces with flap and aileron deflection is formulated. The method is not restricted by the linearized theory assumption and accounts for all standard geometric lifting surface parameters: camber, taper, sweep, washout, dihedral, in addition to flap and aileron deflection. Thickness is not accounted for since the physical lifting body is replaced by a lattice of panels located on the mean camber surface. This panel lattice setup and the treatment of different wake geometries is what distinguish the present work form the overwhelming majority of previous solutions based on the vortex lattice method. A MATLAB code implementing the proposed formulation is developed and validated by comparing our results to existing experimental and numerical ones and good agreement is demonstrated. It is then used to study the accuracy of the widely used classical vortex-lattice method. It is shown that the classical approach gives good agreement in the clean configuration but is off by as much as 30% when a flap or aileron deflection of 30° is imposed. This discrepancy is mainly due the linearized theory assumption associated with the conventional method. A comparison of the effect of four different wake geometries on the values of aerodynamic coefficients was also carried out and it is found that the choice of the wake shape had very little effect on the results.

Keywords—Aileron deflection, camber-surface-bound vortices, classical VLM, Generalized VLM, flap deflection.

I. INTRODUCTION

SINCE Prandtl's lifting line theory is not appropriate for low-aspect-ratio straight wings, swept wings, and so-called delta wings, other aerodynamic models had to be devised in order to predict the aerodynamic characteristics of such plan forms. Among these models is the classical vortex lattice method. The VLM has been in use since the sixties of the twentieth century and is well documented in the literature [1], [2]. It has been applied to the estimation of aerodynamic properties of lifting surfaces and even full airplanes. It belongs to a family of numerical methods which solve potential flow problems on lifting surfaces such as wings, fins, horizontal tails, canards, and even fuselages. These methods replace the actual lifting body with a surface distribution of singular elements (sources, vortices, doublets or a combination of these elements) and apply the tangential flow boundary condition in order to determine the strengths of the singular elements. The Kutta-Joukowski theorem is then applied to determine the

M. Yahyaoui is an associate professor with the Borj El Amri Aviation School, Tunisia and a member of the Applied Mechanics and Systems Laboratory (LASMAP) at the Tunisia Polytechnic School (e-mail: mondher_yahia@yahoo.fr).

aerodynamic coefficients of interest.

The principle of the VLM method is to replace the lifting body with an equivalent lifting surface which is then divided into a grid of trapezoidal panels. To each panel is attached a horseshoe vortex whose bound vortex lies on the quarter-chord of the panel and whose trailing vortices extend downstream to infinity, in a plane that is parallel to the plane of symmetry of the body. In classical VLM solutions based on linearized theory, the vortex-lattice is flat and the trailing vortices extend to infinity in a direction that is either parallel to the lifting body centerline or to the free stream velocity. The flat vortex lattice neglects any displacement of the surface away from the x-y plane which occurs in the wing or wake. This displacement is taken into consideration only in the application of the boundary condition which is imposed on the actual cambered surface.

Some of the most important work applying the classical VLM goes back to 1971 and was developed at NASA [3]. It dealt with complex plan forms which included camber, variable sweep and dihedral, washout, and combinations of wing with either a canard or a tail. A more recent work applying the classical VLM [4] presented a program for estimating aerodynamic characteristics of flapped and twisted plan forms but did not include camber, taper, sweep, nor dihedral.

The approach adopted in the present work is more general than the classical VLM. The panels are placed on the mean camber surface of the body. To each panel is attached a horseshoe vortex with bound vortex segment located at the quarter-chord of the panel. The trailing vortices originating at the endpoints of the bound vortices, initially follow the curvature of the mean camber surface up to the trailing edge, then take a specified downward path (except for an upward deflected aileron) for a certain distance downstream of the trailing edge to eventually be realigned with the free stream velocity. In order to investigate the influence of the wake geometry, four cases of trailing vortices shapes are considered.

A MATLAB code implementing the present generalized approach was developed and used to assess the accuracy of the classical VLM particularly in regard to flap and aileron deflections. The work presented in [5] is some ways similar to the present one but it did not include any control surface deflection. Moreover, the boundary condition applied was of a linearized form and required the addition of the influence of vortex images and the so-called "wave making influences" suitable for hydrofoils. Moreover, they only considered one

World Academy of Science, Engineering and Technology
International Journal of Aerospace and Mechanical Engineering
Vol:8, No:10, 2014

type of wake model, consisting of semi infinite trailing vortices parallel to undisturbed free sea surface.

II. DETAILS OF THE GENERALIZED VORTEX-LATTICE METHOD

In the present work the wing is replaced by a lattice of trapezoidal panels which are superimposed on its mean camber surface. The shape of this surface is defined by airfoil camber, wing aspect ratio, taper, sweep, dihedral, washout, and flap and/or aileron deflection.
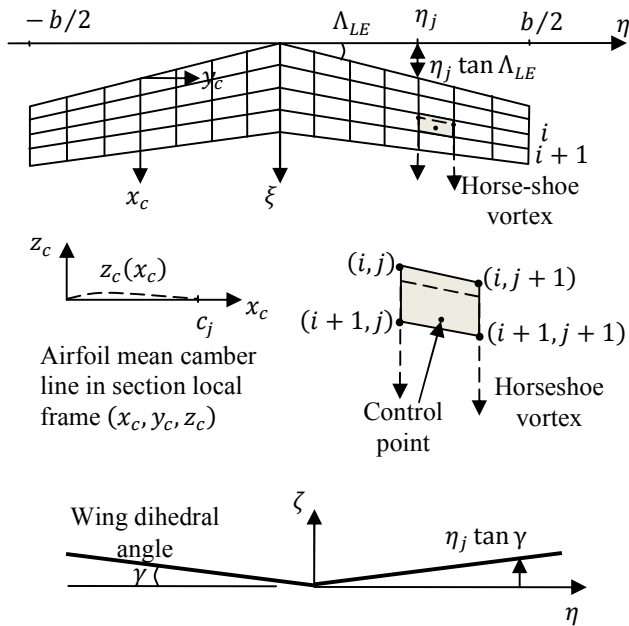

Fig. 1 Wing geometry, panel lattice, horse-shoe vortices, and control points

The coordinates of panel nodes, horse-shoe vortices corner points, and control points will be at first defined by accounting for wing section camber, dihedral, and sweep only. Then a set of rotations will be applied to these coordinates in order to add the effect of washout and flap and/or aileron deflection.

Before the effect of washout or flap and/or aileron deflection is considered, a point on the mean camber surface, situated at a given wing section η, is defined by the following coordinates:

$$\eta_j = -b/2 + (j-1)\Delta\eta \ , \ j = 1, \cdots, N_\eta \tag{1}$$

$$\begin{cases} \xi = \xi_{LE} + x_c = |\eta_j| \tan \Lambda_{LE} + x_c \\ \zeta = \zeta_{LE} + z_c(x_c) = |\eta_j| \tan \gamma + z_c(x_c) \end{cases} \tag{2}$$

where $z_c(x_c)$ defines the shape of the mean camber line of the wing section in its local frame of reference (x_c, y_c, z_c), as shown in Fig. 1. The index LE refers to the wing leading edge.

The effect of washout is now added. It is assumed to vary linearly, from 0° at the centerline to a maximum negative value α_w at wing tip. This corresponds to a constant negative washout gradient:

$$d\alpha/d\eta = 2\alpha_w/b \tag{3}$$

and the change in angle of attack at wing section η_j due to wing washout is given by:

$$\alpha_{w_j} = |\eta_j| \, d\alpha/d\eta \tag{4}$$

Wing twisting is carried out about the leading edge. It affects only (ξ, ζ) coordinates and the changes in these coordinates at the η_j-section are given by:

$$\begin{bmatrix} \xi'_j \\ \zeta'_j \end{bmatrix} = \begin{bmatrix} \xi_{LE_j} \\ \zeta_{LE_j} \end{bmatrix} + \begin{pmatrix} \cos\alpha_{w_j} & \sin\alpha_{w_j} \\ -\sin\alpha_{w_j} & \cos\alpha_{w_j} \end{pmatrix} \begin{bmatrix} \xi_j - \xi_{LE_j} \\ \zeta_j - \zeta_{LE_j} \end{bmatrix} \tag{5}$$

The prime symbol in the above equation does not refer to the first derivative and the washout angle α_w is considered positive here, although it represents a decrease in angle of attack.

Flap and/or aileron deflection also affects the shape of the mean camber surface. Before adding the effect of washout, the (ξ, η)-coordinates of points at flap level are given by (Fig. 2):

$$\begin{cases} \xi \geq \xi_{LE_f} \\ -\left(\eta_{in_f} + b_f\right) \leq \eta \leq -\eta_{in_f} \ or \ \eta_{in_f} \leq \eta \leq \eta_{in_f} + b_f \end{cases} \tag{6}$$

These coordinates, like all points of the lifting surface, first undergo the effect of washout, then the effect of flap deflection. The latter is the result of a rotation of the flap about its leading edge, given by the transformation:

$$\begin{bmatrix} \xi'' \\ \zeta'' \end{bmatrix} = \begin{bmatrix} \xi'_{LE_f} \\ \zeta'_{LE_f} \end{bmatrix} + \begin{pmatrix} \cos\delta_f & \sin\delta_f \\ -\sin\delta_f & \cos\delta_f \end{pmatrix} \begin{bmatrix} \xi' - \xi'_{LE_f} \\ \zeta' - \zeta'_{LE_f} \end{bmatrix} \tag{7}$$

For points on ailerons, a similar transformation is applied but with deflection angle δ_F replaced by δ_a.
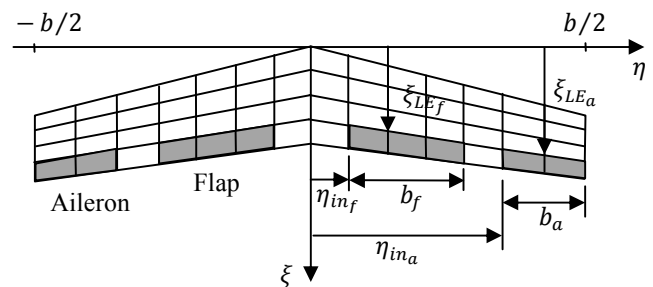

Fig. 2 Definition of flap and aileron geometry

Fig. 3 gives a sample case of a swept wing planform with camber, washout, taper, and dihedral. Flaps and ailerons are also deployed. It also shows samples of horseshoe vortices adhering to the mean camber surface.

To each panel is attached a horseshoe vortex. The bound-vortex segment is located at the panel's quarter-chord, and, as mentioned earlier, the trailing vortices originating at the endpoints of the bound vortex initially follow the curvature of

World Academy of Science, Engineering and Technology
International Journal of Aerospace and Mechanical Engineering
Vol:8, No:10, 2014

the mean camber surface up to the trailing edge, then take a specified downward path (or an upward path for an upward deflected aileron) for a certain distance downstream of the trailing edge, to eventually be realigned with the free stream velocity or any other given direction. A control point is also placed at the three-quarter position on the spanwise center line of each panel. As in the classical VLM, it is at control points that the tangential flow boundary conditions are imposed.

For classical VLM solutions which deal with non planar lifting plan forms, the vortex lattice is flat and lies underneath the actual wing camber surface. The tangential flow boundary condition is on the other hand applied on the mean camber surface itself. Because linearized theory is used in the classical VLM, high accuracy is not expected when flaps and ailerons are deployed at high deflection angles.
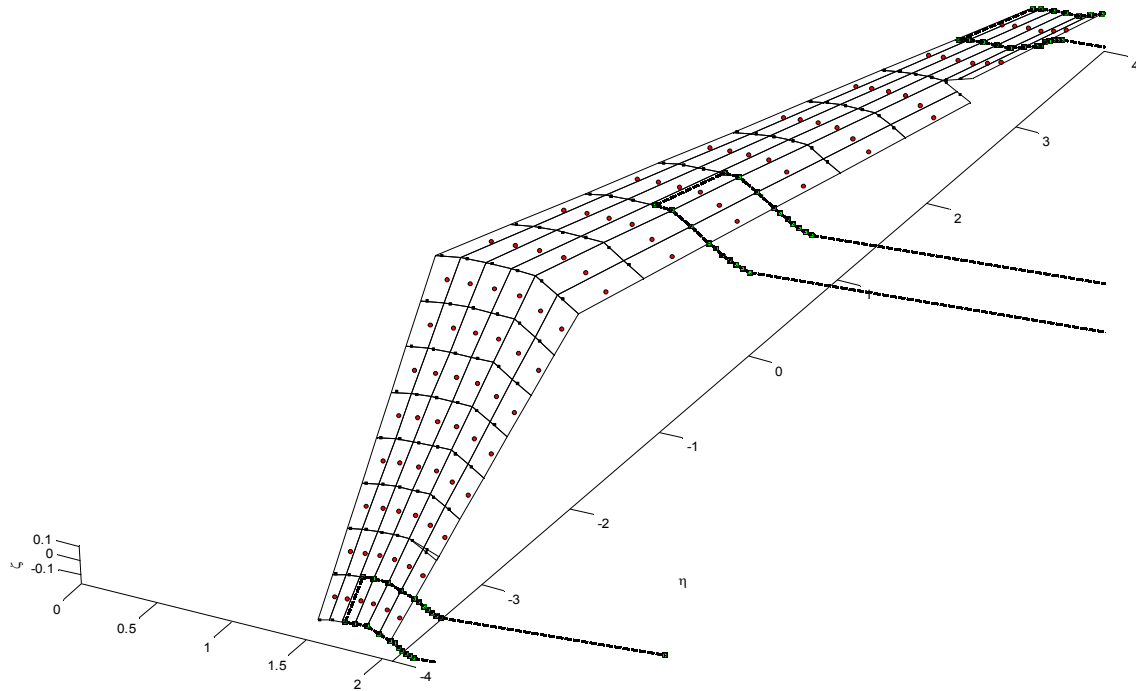

Fig. 3 Mean camber surface with sample curved horseshoe vortices attached to it ($\delta_f = 30°, \delta_a = 20°$)

The velocity induced by the horseshoe vortices on any given control point is computed in the same manner as for the classical VLM, the difference being the number of vortex segments. In the classical VLM, this number is limited to three: the bound vortex and two trailing vortices. In the present generalized method, however, the number of segments is much higher and depends on the chordwise location of the bound vortex, on the lattice resolution, and on the number of points defining the wake. Nonetheless, the same basic formulas associated with the horseshoe vortex given in [1] can still used in the present formulation.

First, what is needed is a general expression of the velocity induced by a finite segment A-B at some control point of coordinates (ξ, η, ζ). So let (ξ_1, η_1, ζ_1) and (ξ_2, η_2, ζ_2) be the coordinates of points A, and B respectively. The desired expression is given by [1]:

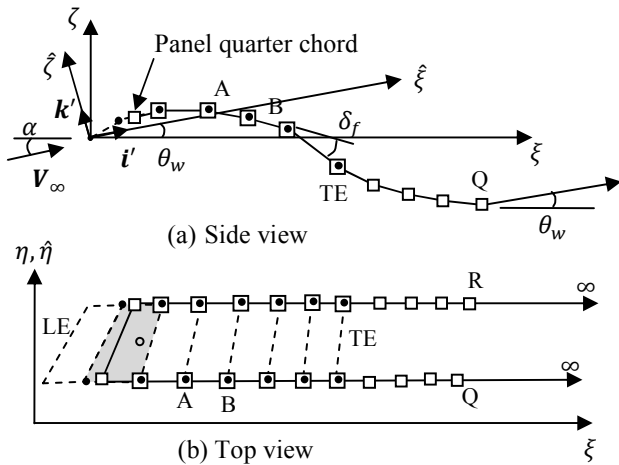$$\boldsymbol{V_{AB}} = \frac{\Gamma_n}{2\pi}\{Fac1_{AB}\}\{Fac2_{AB}\} \qquad (8)$$

where Γ_n is the vortex strength, and:

$$Fac1_{AB} = \{[(\eta - \eta_{1_n})(\zeta - \zeta_{2_n}) - (\eta - \eta_{2_n})(\zeta - \zeta_{1_n})]\boldsymbol{i}$$
$$-[(\xi - \xi_{1_n})(\zeta - \zeta_{2_n}) - (\xi - \xi_{2_n})(\zeta - \zeta_{1_n})]\boldsymbol{j}$$

$$+[(\xi - \xi_{1_n})(\eta - \eta_{2_n}) - (\xi - \xi_{2_n})(\eta - \eta_{1_n})]\boldsymbol{k}\}$$
$$/\{[(\eta - \eta_{1_n})(\zeta - \zeta_{2_n}) - (\eta - \eta_{2_n})(\zeta - \zeta_{1_n})]^2$$
$$+[(\xi - \xi_{1_n})(\zeta - \zeta_{2_n}) - (\xi - \xi_{2_n})(\zeta - \zeta_{1_n})]^2$$
$$+[(\xi - \xi_{1_n})(\eta - \eta_{2_n}) - (\xi - \xi_{2_n})(\eta - \eta_{1_n})]^2\}$$

$$Fac2_{AB} = [(\xi_{2_n} - \xi_{1_n})(\xi - \xi_{1_n}) + (\eta_{2_n} - \eta_{1_n})(\eta - \eta_{1_n})$$
$$+(\zeta_{2_n} - \zeta_{1_n})(\zeta - \zeta_{1_n})]/\sqrt{(\xi - \xi_{1_n})^2 + (\eta - \eta_{1_n})^2 + (\zeta - \zeta_{1_n})^2}$$
$$-[(\xi_{2_n} - \xi_{1_n})(\xi - \xi_{2_n}) + (\eta_{2_n} - \eta_{1_n})(\eta - \eta_{2_n})$$
$$+(\zeta_{2_n} - \zeta_{1_n})(\zeta - \zeta_{2_n})]/\sqrt{(\xi - \xi_{2_n})^2 + (\eta - \eta_{2_n})^2 + (\zeta - \zeta_{2_n})^2}$$

The above equations are good for any bound vortex as well as for the segments that make up the curved part of the trailing vortices, from the endpoints of the bound vortex to points Q and R (Fig. 4). One key restriction on the use of these equations is that the vorticity vector has to be oriented from point A to point B.

World Academy of Science, Engineering and Technology
International Journal of Aerospace and Mechanical Engineering
Vol:8, No:10, 2014

(a) Side view

(b) Top view

□ Vortex segments' end points
● Panel corners

Fig. 4 Side and top views showing the segments which define a typical horseshoe vortex

The contributions of the last portions aft of points Q and R are computed using the formula from the classical VLM for a vortex leg extending to infinity, provided that the frame of reference is rotated around the η-axis in a way that the new abscissa axis points in the prescribed direction of these trailing vortex legs, given by angle θ_w in Fig. 4.

The coordinates of points on these segments as well as those of all control points are first transformed according to the rule:

$$\begin{bmatrix} \hat{\xi} \\ \hat{\eta} \\ \hat{\zeta} \end{bmatrix} = \begin{pmatrix} \cos\theta_w & 0 & \sin\theta_w \\ 0 & 1 & 0 \\ -\sin\theta_w & 0 & \cos\theta_w \end{pmatrix} \begin{bmatrix} \xi \\ \eta \\ \zeta \end{bmatrix} \quad (9)$$

Then the usual formula used in the classical VLM [1] is applied in terms of coordinates in the new rotated frame:

$$\boldsymbol{V'_{Q\infty}} = \frac{\Gamma_n}{2\pi} \left\{ \frac{(\hat{\zeta}-\hat{\zeta}_{1n})\boldsymbol{j}+(\hat{\eta}_{1n}-\hat{\eta})\boldsymbol{k'}}{\left[(\hat{\zeta}-\hat{\zeta}_{1n})^2+(\hat{\eta}_{1n}-\hat{\eta})^2\right]} \right\} \left[1 + \frac{\hat{\xi}-\hat{\xi}_{1n}}{\sqrt{(\hat{\xi}-\hat{\xi}_{1n})^2+(\hat{\eta}-\hat{\eta}_{1n})^2+(\hat{\zeta}-\hat{\zeta}_{1n})^2}} \right] (10)$$

$$\boldsymbol{V'_{R\infty}} = \frac{\Gamma_n}{2\pi} \left\{ \frac{(\hat{\zeta}-\hat{\zeta}_{2n})\boldsymbol{j}+(\hat{\eta}_{2n}-\hat{\eta})\boldsymbol{k'}}{\left[(\hat{\zeta}-\hat{\zeta}_{2n})^2+(\hat{\eta}_{2n}-\hat{\eta})^2\right]} \right\} \left[1 + \frac{\hat{\xi}-\hat{\xi}_{2n}}{\sqrt{(\hat{\xi}-\hat{\xi}_{2n})^2+(\hat{\eta}-\hat{\eta}_{2n})^2+(\hat{\zeta}-\hat{\zeta}_{2n})^2}} \right] (11)$$

The above contributions need to be transferred back to the original (ξ, η, ζ) frame. The backward transformation is simply a rotation in the opposite sense and is given by the equation:

$$\begin{bmatrix} u_{Q\infty} \\ v_{Q\infty} \\ w_{Q\infty} \end{bmatrix} = \begin{bmatrix} -\hat{w}'_{Q\infty}\sin\theta_w \\ v'_{Qw} \\ \hat{w}'_{Q\infty}\cos\theta_w \end{bmatrix} \quad (12)$$

where $\left(0, \hat{v}'_{Q\infty}, \hat{w}'_{Q\infty}\right)$ are the coordinates of $\boldsymbol{V'_{Q\infty}}$ in the rotated frame and $\left(u_{Q\infty}, v_{Q\infty}, w_{Q\infty}\right)$ are those in the wing's original frame.

It's clear that the rotation did not affect the η-component of the induced velocity but has given rise to a ξ-component:

$$u_{Q\infty} = -\frac{\Gamma_n}{2\pi} \frac{(\hat{\eta}_{1n}-\hat{\eta})\sin\theta_w}{(\hat{\zeta}-\hat{\zeta}_{1n})^2+(\hat{\eta}_{1n}-\hat{\eta})^2} \left[1 + \frac{\hat{\xi}-\hat{\xi}_{1n}}{\sqrt{(\hat{\xi}-\hat{\xi}_{1n})^2+(\hat{\eta}-\hat{\eta}_{1n})^2+(\hat{\zeta}-\hat{\zeta}_{1n})^2}} \right] \text{(13-a)}$$

$$v_{Q\infty} = \frac{\Gamma_n}{2\pi} \frac{\hat{\zeta}-\hat{\zeta}_{1n}}{(\hat{\zeta}-\hat{\zeta}_{1n})^2+(\hat{\eta}_{1n}-\hat{\eta})^2} \left[1 + \frac{\hat{\xi}-\hat{\xi}_{1n}}{\sqrt{(\hat{\xi}-\hat{\xi}_{1n})^2+(\hat{\eta}-\hat{\eta}_{1n})^2+(\hat{\zeta}-\hat{\zeta}_{1n})^2}} \right] \text{(13-b)}$$

$$w_{Q\infty} = \frac{\Gamma_n}{2\pi} \frac{(\hat{\eta}_{1n}-\hat{\eta})\cos\theta_w}{(\hat{\zeta}-\hat{\zeta}_{1n})^2+(\hat{\eta}_{1n}-\hat{\eta})^2} \left[1 + \frac{\hat{\xi}-\hat{\xi}_{1n}}{\sqrt{(\hat{\xi}-\hat{\xi}_{1n})^2+(\hat{\eta}-\hat{\eta}_{1n})^2+(\hat{\zeta}-\hat{\zeta}_{1n})^2}} \right] \text{(13-c)}$$

In a similar way, the components of $\boldsymbol{V'_{R\infty}}$ in the wing frame are easily obtained:

$$u_{R\infty} = -\frac{\Gamma_n}{2\pi} \frac{(\hat{\eta}_{2n}-\hat{\eta})\sin\theta_w}{(\hat{\zeta}-\hat{\zeta}_{2n})^2+(\hat{\eta}_{2n}-\hat{\eta})^2} \left[1 + \frac{\hat{\xi}-\hat{\xi}_{2n}}{\sqrt{(\hat{\xi}-\hat{\xi}_{2n})^2+(\hat{\eta}-\hat{\eta}_{2n})^2+(\hat{\zeta}-\hat{\zeta}_{2n})^2}} \right] \text{(14-a)}$$

$$v_{R\infty} = \frac{\Gamma_n}{2\pi} \frac{\hat{\zeta}-\hat{\zeta}_{2n}}{(\hat{\zeta}-\hat{\zeta}_{2n})^2+(\hat{\eta}_{2n}-\hat{\eta})^2} \left[1 + \frac{\hat{\xi}-\hat{\xi}_{2n}}{\sqrt{(\hat{\xi}-\hat{\xi}_{2n})^2+(\hat{\eta}-\hat{\eta}_{2n})^2+(\hat{\zeta}-\hat{\zeta}_{2n})^2}} \right] \text{(14-b)}$$

$$w_{R\infty} = \frac{\Gamma_n}{2\pi} \frac{(\hat{\eta}_{2n}-\hat{\eta})\cos\theta_w}{(\hat{\zeta}-\hat{\zeta}_{2n})^2+(\hat{\eta}_{2n}-\hat{\eta})^2} \left[1 + \frac{\hat{\xi}-\hat{\xi}_{2n}}{\sqrt{(\hat{\xi}-\hat{\xi}_{2n})^2+(\hat{\eta}-\hat{\eta}_{2n})^2+(\hat{\zeta}-\hat{\zeta}_{2n})^2}} \right] \text{(14-c)}$$

The total velocity induced by the horseshoe vortex from panel n at control point on panel m is obtained by summing the contribution from all the finite segments, as given by (8), and from the two semi infinite segments, "Q∞" and "R∞", as given by (13) and (14). The result can be written if the form:

$$\boldsymbol{V_{m,n}} = \boldsymbol{C_{m,n}}\Gamma_n \quad (15)$$

The overall velocity induced at control point m by all the horseshoe vortices is:

$$\boldsymbol{V_{m_i}} = \sum_{n=1}^{N} \boldsymbol{C_{m,n}}\Gamma_n = u_{m_i}\boldsymbol{i} + v_{m_i}\boldsymbol{j} + w_{m_i}\boldsymbol{k} \quad (16)$$

III. BOUNDARY CONDITION

The strengths of the bound vortices are obtained, as for the classical VLM, by application of the tangential flow boundary condition at the cambered surface, specifically at control points located at the three quarter chord position in the spanwise center line of each panel. This boundary condition means that the total velocity at control point m has no component normal to the lifting surface at that point.

The lifting surface can be modeled by the equation:

$$z = f(\xi, \eta) \quad (17)$$

Rewrite the above equation in the form:

$$F(\xi, \eta, \zeta) = \zeta - f(\xi, \eta) = 0$$

World Academy of Science, Engineering and Technology
International Journal of Aerospace and Mechanical Engineering
Vol:8, No:10, 2014

Then the boundary condition can be modeled by the equation:

$$\boldsymbol{V_m} \cdot (\boldsymbol{\nabla} F)_m = 0 \qquad (18)$$

where $\boldsymbol{\nabla} F$ is the gradient of function F. It is normal to the surface at any control point m:

$$(\boldsymbol{\nabla} F)_m = -\left(\frac{\partial f}{\partial \xi}\right)_m \boldsymbol{i} - \left(\frac{\partial f}{\partial \eta}\right)_m \boldsymbol{j} + \boldsymbol{k} \qquad (19)$$

Or the total velocity at any control point is the sum of $\boldsymbol{V}_{m_i}$, given by (16), and the free stream velocity which is:

$$\boldsymbol{V_\infty} = \boldsymbol{i} V_\infty \cos\alpha + \boldsymbol{k} V_\infty \sin\alpha \qquad (20)$$

where α is the local section angle of attack, at the spanwise location of point m. So the total velocity is:

$$\boldsymbol{V_m} = (V_\infty \cos\alpha + u_{m_i})\boldsymbol{i} + v_{m_i}\boldsymbol{j} + (V_\infty \sin\alpha + w_{m_i})\boldsymbol{k} \quad (21)$$

Substituting (19) and (21) into (18) and using (16) leads to the following equation:

$$-\left(\frac{\partial f}{\partial \xi}\right)_m \left(V_\infty \cos\alpha + \sum_{n=1}^N C_{m,n_i}\Gamma_n\right) - \left(\frac{\partial f}{\partial \eta}\right)_m \left(\sum_{n=1}^N C_{m,n_j}\Gamma_n\right) + \left(V_\infty \sin\alpha + \sum_{n=1}^N C_{m,n_k}\Gamma_n\right) = 0$$

Collecting the terms containing the vortex strengths, a linear system of algebraic equations is obtained:

$$\sum_{n=1}^N \left[C_{m,n_k} - \left(\frac{\partial f}{\partial \xi}\right)_m C_{m,n_i} - \left(\frac{\partial f}{\partial \eta}\right)_m C_{m,n_j}\right]\Gamma_n = V_\infty\left[\left(\frac{\partial f}{\partial \xi}\right)_m \cos\alpha - \sin\alpha\right] \quad (22)$$

for $m = 1, \dots, N$.

Equation (22) is the basis of the solution of the generalized VLM problem. The details behind the computations of $\partial f / \partial \xi$ and $\partial f / \partial \eta$ in this equation are rather lengthy and it is left to the reader to develop these derivatives.

Once the vortex strengths are obtained, various aerodynamic coefficients can be obtained by means of the Kutta-Joukowski theorem [1], [3]. The lift and induced drag coefficients are computed according to the equations:

$$C_L = \frac{2AR}{b^2 V_\infty^2}\sum_{k=1}^{N_p}(V_\infty + \tilde{u}_k)\Gamma_k \Delta\eta_k \qquad (23)$$

$$C_{D_i} = -\frac{2AR}{b^2 V_\infty^2}\sum_{k=1}^{N_p}\tilde{w}_k \Gamma_k \Delta\eta_k \qquad (24)$$

While the pitching moment coefficient at the mean aerodynamic center, and the rolling moment coefficients are given by:

$$C_{m_{ac}} = \frac{2AR}{\bar{c}b^2 V_\infty^2}\sum_{k=1}^{N_p}(\xi_{ac} - \xi_k)(V_\infty + \tilde{u}_k)\Gamma_k \Delta\eta_k \qquad (25)$$

$$C_l = -\frac{2AR}{b^3 V_\infty^2}\sum_{k=1}^{N_p}\eta_k (V_\infty + \tilde{u}_k)\Gamma_k \Delta\eta_k \qquad (26)$$

In the above equations, ξ_k and η_k are the coordinates of the centers of the bound vortices and $(\tilde{u}_k, \tilde{v}_k, \tilde{w}_k)$ are the overall induced velocity components at those centers and not at the control points. The coordinate of the mean aerodynamic center is given by:

$$\xi_{ac} = \frac{c_o}{4} + \frac{1 + 2\sigma}{1 + \sigma}\frac{b}{6}\tan\Lambda_{LE}$$

where c_0 is the wing centerline chord.

IV. Validation

A. An Example from Bertin and Smith

Reference [1] gives the lift coefficient as a function of angle of attack for a wing with an aspect ratio of 5, a taper ratio of unity, an uncambered section, and a 45° sweep angle. The corresponding lift-curve slope is:

$$C_{L_\alpha} = 3.443/rad$$

With an identical lattice, the present code gives:

$$C_{L_\alpha} = 3.4416/rad$$

The two values are almost identical. The relative difference between them is 0.04%.

B. An Example from NACA TN N°1270

Reference [6] presents the results of an experimental study of seven wings of NACA 44-series sections, with aspect ratios of 8, 10, and 12 and taper ratios of 0.4 and 0.286. The wings were also twisted but had neither dihedral nor sweep at the quarter-chord line.

Among these wings, one with an aspect ratio of 8, a taper ratio of 0.4 and a washout of -4.5° is considered for comparison. This wing also had a thickness-to-chord ratio varying from 16% at the root to 12% at wing tip. This geometric property was not taken into consideration since the VLM does not account for section thickness. Instead, the NACA 4415 was taken over the entire span.

A lattice of 8 chordwise rows and 40 spanwise rows of panels was used. Values for the lift curve slope, maximum lift-to-drag ratio, and zero-lift angle of attack are compared to experimental ones and overall good agreement is obtained as shown in Fig. 5 and Table I.

When computing the maximum lift-to-drag ratio, since the VLM gives only the induced drag coefficient, the profile drag coefficient was directly read from the experimental drag polar given in [9], at an angle of attack of 3°. This is the angle of attack yielding the highest value of L/D.

C. An Example from NASA TN D-6142

Among the cases studied in [3] is a 45° swept wing with aspect ratios of 7 and a taper ratio of 1. The lift curve slope is computed for different values of the number of panels per half span (N_S) and compared to values given in that reference. The results are presented in Fig. 6 and again good agreement is obtained.
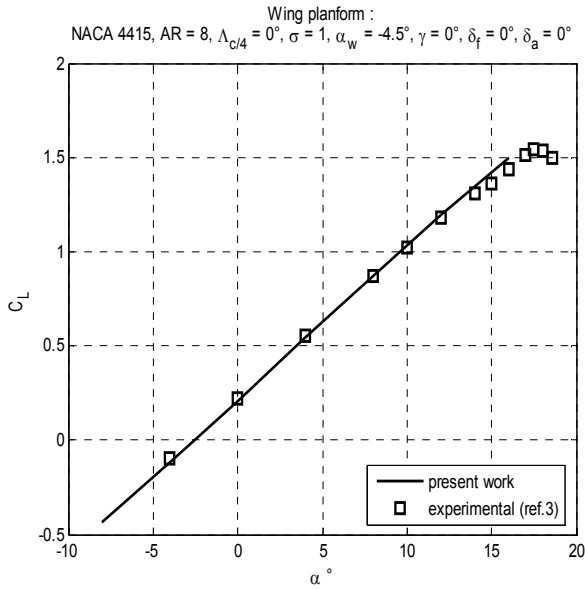
World Academy of Science, Engineering and Technology
International Journal of Aerospace and Mechanical Engineering
Vol:8, No:10, 2014

Fig. 5 Lift curve for the tapered and twisted wing

TABLE I
COMPARISON OF PRESENT WORK RESULTS TO EXPERIMENTAL ONES

Variable	C_{L_α}	$(L/D)_{max}$	$\alpha_{L=0}(°)$
Reference value	0.082	27.8	-2.9
Present work	0.084	28.2	-2.81
% difference	2	1	3
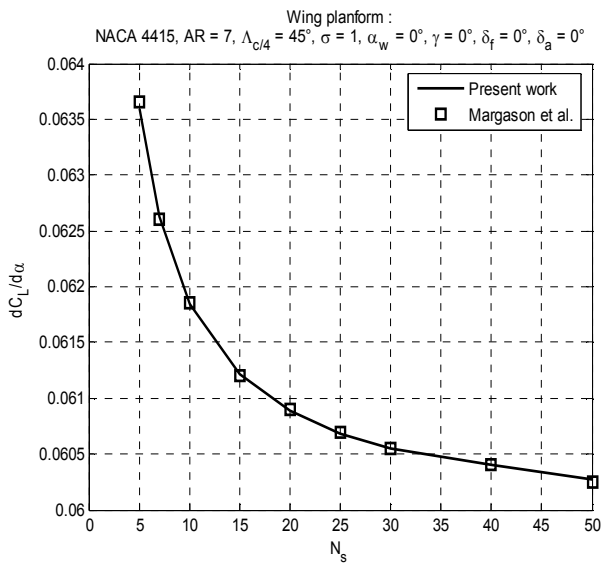
Fig. 6 Comparison of values of C_{L_α} to those from [3]

D. Evaluating Flap Effectiveness

In order to check the accuracy of the generalized VLM code in determining flap effectiveness, a reference value for the derivative $C_{L_{\delta_f}}$ is computed manually according to the procedure outlined in [7], [8] which uses the equation:

$$C_{L_{\delta_f}} = K_b \, C_{l_{\delta_f}} \left(\frac{C_{L_\alpha}|_M}{C_{l_\alpha}|_M} \right) \left(\frac{\alpha_{\delta_f}|_{C_L}}{\alpha_{\delta_f}|_{C_l}} \right) \qquad (27)$$

where:
- Coefficient K_b is the flap span factor
- $C_{l_{\delta_f}}$ is the increase in section lift coefficient with flap deflection
- $C_{L_\alpha}|_M$ and $C_{l_\alpha}|_M$ are the lift-curve slopes of the wing and wing section, respectively, at the given Mach number
- $\alpha_{\delta_f}|_{C_L} / \alpha_{\delta_f}|_{C_l}$ is the ratio of three-dimensional flap-effectiveness parameter to two-dimensional flap-effectiveness parameter

It can easily be checked that, for a rectangular wing with aspect ratio of 8, with no dihedral nor washout, and for which the trailing edge flap covers the whole span and 25% of the chord, the outlined procedure gives a value for $C_{L_{\delta_f}}$ around 0.052 per degree. The value provided by the generalized VLM code is 0.054 per degree. The relative difference between the two values is 4%.
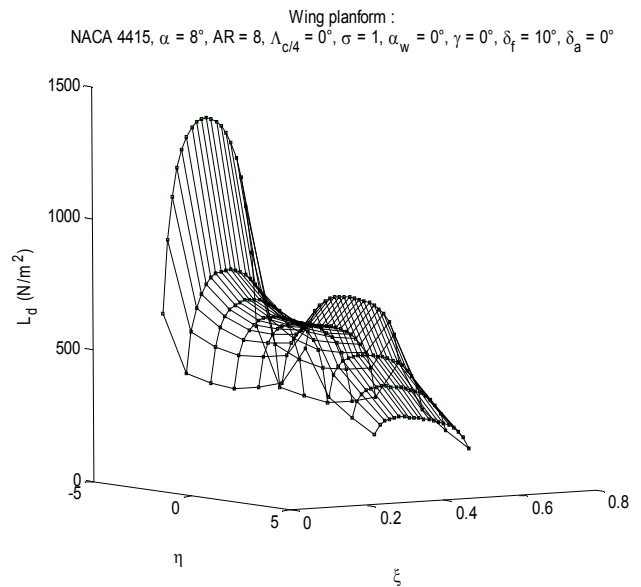

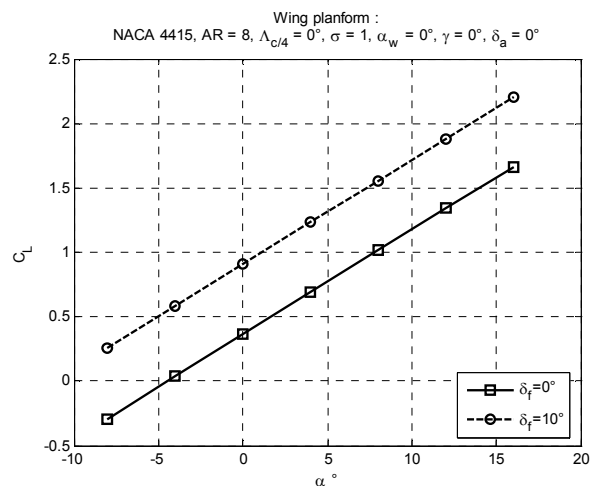Fig. 7 Lift distribution over a wing planform with 10° flap deflection

Fig. 8 Effect of a 10° flap deflection on the lift curve

World Academy of Science, Engineering and Technology
International Journal of Aerospace and Mechanical Engineering
Vol:8, No:10, 2014

V. ACCURACY CHECK OF THE CLASSICAL VLM FOR FLAP AND AILERON DEFLECTION

The purpose in this section is to evaluate the accuracy or limitations of the widely used classical VLM, which based on linearized theory, in modeling flap and aileron deployment. For this purpose, a separate MATLAB code implementing the classical version of the VLM was also developed.

Since any drawbacks that might be expected in regard to the classical VLM would most likely arise from the linearized theory approach, flaps and ailerons should be deployed at important angles for any limitations to appear. Therefore, deflections angles up to 30° are imposed and values for aerodynamic coefficients such as lift coefficient (C_L), pitching moment coefficient at the aerodynamic center ($C_{m_{ac}}$), and rolling moment coefficient (c_l) are compared.

Numerical results for a rectangular wing an aspect ratio of 8 and a washout of -4° are given in Fig. 9 and 10. A lattice of 8 chordwise rows and 20 spanwise rows of panels was used. Coefficients C_L and $C_{m_{ac}}$ are drawn as functions of flap deflection angle, with the flap span equal to that of the wing and its chord occupying 25% of the wing chord. The results show that the classical vortex-lattice method does not give accurate values for the aerodynamic coefficients for flap deflection angles higher than 10°. There is a 24% relative error in the lift coefficient and a 30% error in pitching moment coefficient at the mean aerodynamic center for a flap deflection angle of 30°.

The rolling moment coefficient and $C_{m_{ac}}$ are computed as a function of aileron deflection. The results presented in Fig. 11 and 12 correspond to the same rectangular wing of the previous case, but with ailerons deflected instead of flaps. The ailerons have a chord ratio of 25%, a span ratio of 40% and their outer edge at wing tip. Coefficients $C_{m_{ac}}$ and C_l are plotted and the results show that the classical VLM lacks accuracy for aileron deflection angles greater than 10°. The discrepancy in C_l is about 30% for a 30° aileron angle.
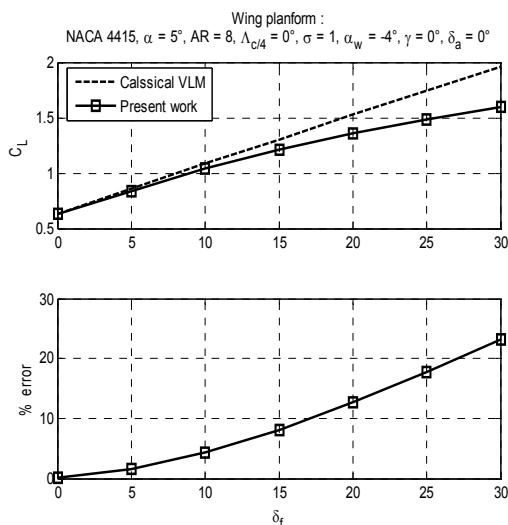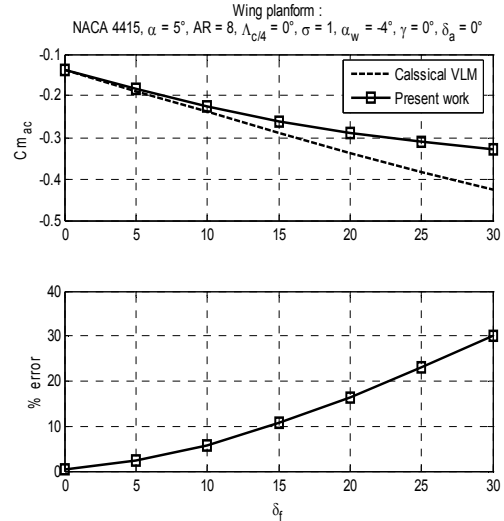

Fig. 10 Classical VLM: error in $C_{m_{ac}}$ as a function of flap deflection

Overall, the classical VLM has proven to be highly accurate when no flap or aileron is deployed. The numerical values given by this method are within 1% of the ones provided by the generalized VLM. The classical VLM is more than adequate when dealing with normal wing geometric parameters such as section camber, taper, washout, sweep, and dihedral. But the advantage the generalized VLM has is that it can accurately handle mobile surface deflection at high angles.

All the results presented so far are based on the wake condition shown in Fig. 4 with $\theta_w = \alpha$. Vortex legs leaving the wing the trailing edge are initially curved and then become straight and parallel to the free stream velocity. Such choice is believed to give better results than other frequently used wake models [2] and has proven its accuracy in our computations. Nonetheless, an investigation of the effect of wake geometry on the values of the aerodynamic coefficients is worth considering. This is done in the following section.
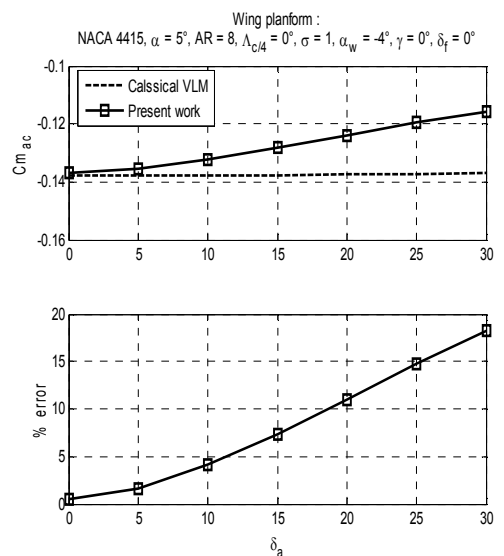

Fig. 9 Classical VLM: error in lift coefficient as function of flap deflection

Fig. 11 Classical VLM: error in $C_{m_{ac}}$ as a function of aileron deflection

World Academy of Science, Engineering and Technology
International Journal of Aerospace and Mechanical Engineering
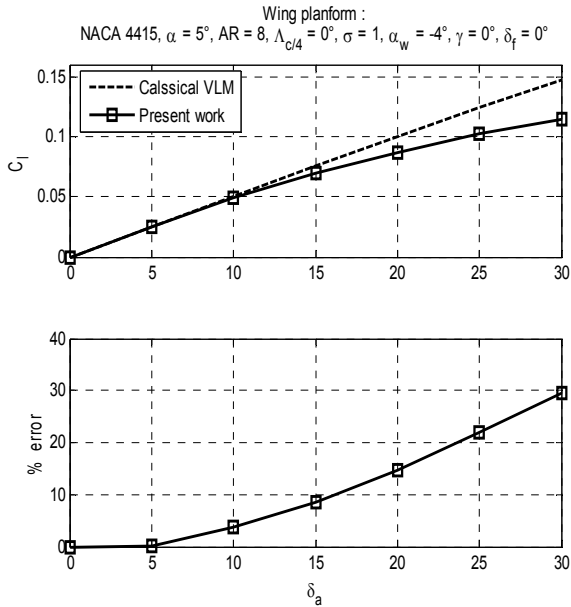Vol:8, No:10, 2014

Fig. 12 Classical VLM: error in rolling moment coefficient as a function of aileron deflection

VI. Effect of Wake Geometry

In order to investigate the dependence of the solution on wake shape, four different cases are considered (Fig. 13):
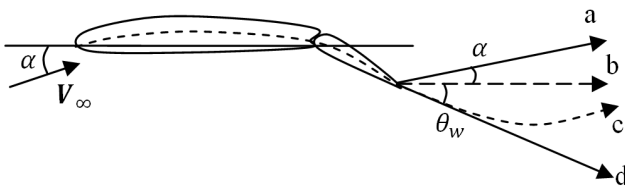

Fig. 13 Prescribed wake shapes

- Shape (a): the trailing vortex legs leave the trailing edge as straight segments extending to infinity parallel to the free stream velocity.
- Shape (b): the trailing vortex legs leave the trailing edge as straight segments extending to infinity parallel to the wing centerline.
- Shape (c): the vortex legs follow a curved path whose initial slope is that of the mean camber line at the trailing edge, then become straight an parallel to the free stream velocity.
- Shape (d): the trailing vortex legs leave the trailing edge as straight segments extending to infinity having the slope of the mean camber line at the trailing edge.

The four different wake shapes are applied to the previously considered wing with aspect ratio of 8, a taper ratio of 0.4, a washout of -4.5° and no dihedral or sweep at the quarter chord [6]. A lattice of 10 chordwise rows and 40 spanwise rows of panels was used in computing the lift coefficient and lift-to-drag ratio at an angle of attack of 4°. The results corresponding to the four wake geometries are given in Table II along with reference experimental ones. All the computed

values are within a margin of less than 1% of the reference experimental values. These results show that the wake geometry has practically no effect on the aerodynamic coefficients.

TABLE II
EFFECT OF WAKE SHAPES ON KEY AERODYNAMIC COEFFICIENTS

Wake shape	a	b	c	d	Experimental [6]
C_L	0.539	0.538	0.539	0.537	0.54
L/D	27.71	27.73	27.81	27.84	27.8

VII. Conclusion

A generalized VLM where the lattice takes the shape of the wing mean camber surface and which does not adopt the linearized theory approach has been formulated. A MATLAB code, implementing this formulation, has been developed and validated by comparing computational results to several cases of published numerical and experimental values. A second code implementing the classical vortex lattice method based on linearized theory was developed and an evaluation of the accuracy of the classical method was carried out by comparing values given by the two codes. It is shown that the classical vortex lattice method gives good results for plan forms with standard values of dihedral, washout, taper, and twist in the clean configuration. It has also proven to be fairly accurate for low flap and aileron deflection angles not exceeding 10°. However, a relative error of 30% in rolling moment coefficient is recorded at an aileron deflection of 30° and an error of 24% in lift coefficient is obtained at a 30° flap deflection angle. These errors are attributed to the linearized theory approach upon which is based the classical vortex lattice method. The effect of wake geometry on key aerodynamic coefficients was also studied and the findings indicate that the wake geometry had little effect on these coefficients.

The accuracy of the generalized vortex lattice method presented in this paper makes it very useful in aerodynamic studies dealing with control surface deflection such as the study of longitudinal static stability and control of wing-horizontal tail or Canard-wing-horizontal tail combinations. An extension of the present code which would allow for such lifting surface combinations is being considered. An immediate and easier extension of the present work is to allow for variable sweep and washout, and in particular, the study of localized twist near the wing tip instead of twisting the whole wing. The newly formulated method can also be used to provide numerical data for parameters such as Oswald efficiency factor and variation of downwash angle with angle of attack for wings with complex geometries and mobile surface deflection. It can also be oriented toward the computation of a number of stability derivatives by allowing the wing or wing-stabilizer combination to pitch, yaw, and roll.

References

[1] Bertin, J.J., and Smith, M.L. *Aerodynamics for engineers*, 3rd Ed, Prentice Hall, 1998.

[2] Katz, J., and Plotkin A., *Low-speed aerodynamics*, McGraw-Hill Books Co., 1991.

[3] Margason, R.J., and Lamar, J.E., "Vortex-Lattice FORTRAN Program for Estimating Subsonic Aerodynamic Characteristics of complex plan forms," NASA TN D66142, 1971.

[4] Donaldon, M.V., and Mueller de Almeida, S.F.," A vortex lattice program for steady state aerodynamic analysis of flapped and twisted uav wing plan forms", Brazilian symposium on Aerospace Engineering & Applications, 2009.

[5] Thiart, G.D., "Generalized vortex lattice method for prediction hydrofoil characteristics", *R&D Journal*, 2001.

[6] Neely, R.H., Bollech, T.V., Westrick, J.C., and R.R. Graham, "Experimental and calculated characteristics of several NACA 44-series wings with aspect ratios of 8, 10, and 12 and taper ratios of 2.5 and 3.5", NACA TN 1270, 1947.

[7] J. Roskam, *Methods for estimating stability derivatives of conventional subsonic aircraft*, 1971.

[8] Lowry, G.J., and Polhamus, E.C., "A method for predicting lift increment due to flap deflection at low angle of attack in incompressible flow", NACA TN 3911, 1957.

[9] Abbott, I.H., and Von Doenhoff, A.E., *Theory of wing sections*, Dover Publications, 1959.